Extreme Mechanics Letters 17 (2017) 16–23

Contents lists available at ScienceDirect

Extreme Mechanics Letters

journal homepage: www.elsevier.com/locate/eml

# Elastic behaviour at the nanoscale of innovative composites of nanoporous gold and polymer

Emma Griffiths [a,*], Swantje Bargmann [b], B.D. Reddy [a]

[a] Centre for Research in Computational and Applied Mechanics, University of Cape Town, South Africa
[b] Chair of Solid Mechanics, University of Wuppertal, Germany

ARTICLE INFO

*Article history:*
Received 25 August 2017
Received in revised form 19 September 2017
Accepted 19 September 2017
Available online 27 September 2017

*Keywords:*
Nanocomposite
Homogenization
Micromechanics
Hierarchical materials

ABSTRACT

Nanoporous gold is a material with unique properties that make it attractive for use in multiple areas. It has an extremely high compressive strain capability but is very brittle in tension which limits its usage. One means of addressing this limitation is to fill the voids of the nanoporous material with a polymer, resulting in a more ductile and stronger material. In this work, the mechanical properties of a nanocomposite representative sample are studied numerically. The study is based on homogenization with the use of three types of boundary conditions. The stress–strain response within the composite is also analysed. Under a pure compression test, the sample shows both compressive and tensile strains and stresses. This is due to the complex interaction within the microstructure. Within the composite, the polymer is still considerably more compliant than the gold material showing much higher strains. The resultant forces, moments and torques acting on representative ligament cross-sections are also investigated under compressive loading. Bending moments and normal forces dominate the modes of loading. Ligaments along the compression axis show markedly higher normal forces compared to ligaments perpendicular to this axis. The normal stress distributions of the ligaments show clear trends towards combined bending and normal forces while there is no discernible pattern to the shear stress distributions. These nevertheless generate high shear forces and torques.



## 1. Introduction

Nanoporous metals generally exhibit different and appealing properties compared to their bulk counterparts. A key example is nanoporous gold, which is obtained from a dealloying process, and which comprises a material of up to $10^{15}$ metal nano-ligaments per cubic centimetre connected within a continuous network (Fig. 1).

Newly developed composites of nanoporous gold and polymer have raised large interest. The nanoporous gold has a bicontinuous microstructure and is based on interconnected metallic ligaments which behave as ultra high-strength nanowires [2] and constitute the main load carrying phase. Moreover, nanoporous gold possesses an unconventionally high strength-to-porosity ratio [3] due to a high surface-to-volume ratio and shows a direct relationship between the volume fraction and the yield strength [4], while an inverse relationship exists between the ligament diameter size and macroscopic mechanical properties [5,3]. Such distinctive properties render it a promising candidate for use in areas such as catalysis [6,7], sensing [8] and actuation [9].

An uncommon feature of nanoporous gold compared to other nanoporous metals is its very high ductility in compression with strains of up to 200% without macroscopic fracture being reported [10,5]. However, it exhibits extreme brittleness in tension [11,10,12,13]. This is a limiting factor in its use in structural applications. To improve the mechanical properties, the creation of a superior nanocomposite through the addition of a polymer into the voids of nanoporous gold has been suggested by Wang and Weismüller [4]. This composite exhibits favourably unique features. Most importantly, the nanocomposite shows high tensile ductility with no apparent fracture under bending tests. The compressive ductility is also retained. Furthermore, the hardness value and yield strength of the composite are greater than either constituent. A direct relationship between ligament size and yield strength is also observed.

The mechanism causing the improved ductility of the nanocomposite is still unknown, though the ductility of the ligaments is suggested as a major factor [5,12]. Examining the ligaments within pure nanoporous gold under compression, Huber et al. [14] observed bending to be the main loading case for the ligaments while tension/compression effects were less evident. A change in the loading case of the ligaments may create the distinct features of greater strength and hardness values and the tensile ductility

* Corresponding author.
*E-mail addresses:* GRFEMM002@myuct.ac.za (E. Griffiths), bargmann@uni-wuppertal.de (S. Bargmann), daya.reddy@uct.ac.za (B.D. Reddy).

https://doi.org/10.1016/j.eml.2017.09.006

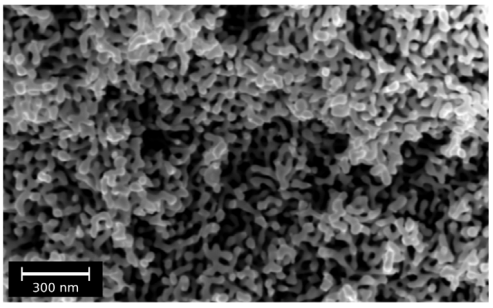


**Fig. 1.** Scanning electron micrograph of nanoporous gold showing the interconnected network resulting in a high surface area-to-volume ratio. Ligament diameter of ca. 30 nm. Reprinted from Wilmers et al. 2017 [1].
*Source:* Image courtesy of Nadiia Mameka at Helmholtz-Zentrum Geesthacht.


of the composite. Greater axial elongation and shortening of the gold ligaments in the composite were noted under experimental observation by Wang and Weismüller [4] suggesting deformation is dominated by tension/compression. The tension/compression dominated behaviour was suggested as a factor to account for the increased strength in the composite as this requires larger local stresses to occur in the ligaments for the onset of deformation compared to bending dominated behaviour [4]. Numerical compression tests on a simplified two-dimensional periodic honeycomb model of the composite showed that ligaments experience a compressive stress response if they are aligned along the compression axis [15]. Ligaments not along this axis show both a compressive and bending response. The simplicity of the model, however, has limited the extent to which conclusions about the response could be drawn. A more realistic, and therefore complex, model is needed to explore computationally the details of the behaviour of the gold–polymer nanocomposite. In tensile tests of pure nanoporous gold the ligaments showed necking suggesting significant tension/compression loading modes present [10,12]. The exploration of the ligament deformation mode of the composite under tension has not been extensively investigated.

This work reports on the homogenization of a gold–polymer nanocomposite RVE using the finite element method. The calculated elasticity tensor reveals an almost isotropic material. The effective shear modulus, bulk modulus, Young's modulus and Poisson's ratio are determined under kinematic uniform, static uniform and periodic boundary conditions. The elastic response and loading case of the different constituents in the material are investigated by studying the principal stresses and strains along the centroid as well as the mechanical stress response of individual ligaments within the composite under compression testing. Although pure nanoporous gold shows a tension–compression asymmetry [16,17], the composite RVE showed a symmetric tension–compression elastic response and thus only compression loading will be investigated here. The normal and shear stress distribution of the cross section of several ligaments enables us to observe the dominant loading case of the gold ligaments which may include bending, pure compression or tension, torsion, or shear stress.

## 2. Theory

### 2.1. Homogenization problem

Consider a linear elastic body which occupies a domain $\bar{\mathrm{V}}$. The body is assumed to undergo small deformations with the infinitesimal strain being given in terms of the displacement by

$$\boldsymbol{\varepsilon}(\boldsymbol{u}) = \frac{1}{2}\left[\nabla\boldsymbol{u} + [\nabla\boldsymbol{u}]^{\mathrm{T}}\right], \tag{1}$$

where $\boldsymbol{u}$ is the displacement field.

The constitutive relation for the material is given by

$$\boldsymbol{\sigma} = \mathbb{C} : \boldsymbol{\varepsilon}, \tag{2}$$

where $\boldsymbol{\sigma}$ and $\boldsymbol{\varepsilon}$ are respectively the Cauchy stress and infinitesimal strain tensors and $\mathbb{C}$ is the elasticity tensor. Most generally, $\mathbb{C}$ has 21 independent components, but for the special case of an isotropic material this reduces to two independent constants, for example, the bulk modulus $\kappa$ and shear modulus $\mu$. In this case Eq. (2) takes the form

$$\boldsymbol{\sigma} = \kappa\,[\mathrm{tr}\boldsymbol{\varepsilon}]\,\boldsymbol{I} + 2\mu\boldsymbol{\varepsilon}'. \tag{3}$$

Here $\mathrm{tr}\boldsymbol{\varepsilon}$ denotes the trace of the strain and $\boldsymbol{\varepsilon}' \overset{\text{def}}{=} \boldsymbol{\varepsilon} - \frac{\mathrm{tr}\boldsymbol{\varepsilon}}{3}\boldsymbol{I}$ is the strain deviator.

For the purpose of carrying out a homogenization analysis, the domain under consideration is a representative sample of the bulk domain, and referred to as an RVE with volume V. The RVE comprises two linear elastic materials, labelled 1 and 2, with material 1 having volume fraction $\varphi$. The domains $\mathrm{V}_1$ and $\mathrm{V}_2$ comprising the two materials are individually homogeneous and non-penetrating, so that $\mathrm{V}_1 \cap \mathrm{V}_2 = \varnothing$. The boundary of the RVE is denoted by $\partial\mathrm{V}$ and comprises two non-overlapping parts $\partial\mathrm{V}_u$, on which displacements are given by $\boldsymbol{u} = \bar{\boldsymbol{u}}$, and $\partial\mathrm{V}_t$, on which the tractions are given by $\boldsymbol{t} = \bar{\boldsymbol{t}}$.

With a body force $\mathbf{f}$, the weak form of the equilibrium problem for the heterogeneous elastic body is as follows: Find $\boldsymbol{u} \in \vee$ such that $\boldsymbol{u} = \bar{\boldsymbol{u}}$ on $\partial\mathrm{V}_u$ and

$$\int_{\mathrm{V}} \nabla\mathbf{w} : \mathbb{C} : \boldsymbol{\varepsilon}(\boldsymbol{u})\mathrm{dV} = \int_{\mathrm{V}} \mathbf{f}\cdot\mathbf{w}\mathrm{dV} + \int_{\partial\mathrm{V}_t} \boldsymbol{t}\cdot\mathbf{w}\mathrm{d}A \qquad \forall\mathbf{w} \in \vee, \tag{4}$$

where $\vee$ is the test space of functions which together with their first derivatives are square-integrable, and which satisfy $\mathbf{w} = \mathbf{0}$ on $\partial\mathrm{V}_u$.

The objective is to obtain an effective elasticity tensor $\mathbb{C}^*$ for the RVE that relates the volume-averaged stress $\langle\boldsymbol{\sigma}\rangle_{\mathrm{V}}$ to the volume-averaged strain $\langle\boldsymbol{\varepsilon}\rangle_{\mathrm{V}}$ given by

$$\langle\boldsymbol{\sigma}\rangle_{\mathrm{V}} = \mathbb{C}^* : \langle\boldsymbol{\varepsilon}\rangle_{\mathrm{V}}, \tag{5}$$

that relates the volume-averaged stress $\langle\boldsymbol{\sigma}\rangle_{\mathrm{V}}$ to the volume-averaged strain $\langle\boldsymbol{\varepsilon}\rangle_{\mathrm{V}}$ where $\langle\cdot\rangle_{\mathrm{V}} \overset{\text{def}}{=} \frac{1}{|\mathrm{V}|}\int_{\mathrm{V}} \cdot\,\mathrm{dV}$. This relation must be valid for bodies in equilibrium, which furthermore must satisfy the Hill–Mandel criterion [18], in terms of which the product of the average stress and strain is equal to the actual internal work

$$\langle\boldsymbol{\sigma}\rangle : \langle\boldsymbol{\varepsilon}\rangle = \frac{1}{|\mathrm{V}|}\int_{\mathrm{V}} \boldsymbol{\sigma} : \boldsymbol{\varepsilon}\mathrm{dV}.$$

There are three types of boundary conditions for which the Hill–Mandel condition [18] is valid: kinematic uniform (KU), static uniform (SU) and periodic (P). These are defined by

$$\begin{aligned}
&\text{kinematic uniform:} && \boldsymbol{u}|_{\partial\mathrm{V}} = \mathcal{E}\cdot\mathbf{x} \\
&&& \text{where } \langle\boldsymbol{\varepsilon}\rangle_{\mathrm{V}} = \mathcal{E} \text{ and } \partial\mathrm{V} = \partial\mathrm{V}_u, && \text{(6a)}\\
&\text{static uniform:} && \boldsymbol{t}|_{\partial\mathrm{V}} = \mathcal{L}\cdot\mathbf{n} \\
&&& \text{where } \langle\boldsymbol{\sigma}\rangle_{\mathrm{V}} = \mathcal{L} \text{ and } \partial\mathrm{V} = \partial\mathrm{V}_t, && \text{(6b)}\\
&\text{periodic:} && \boldsymbol{u}|_{\partial\mathrm{V}} = \mathcal{E}\cdot\mathbf{x} + \boldsymbol{v}, \\
&&& \text{where } \boldsymbol{v} \text{ is a fluctuation.} && \text{(6c)}
\end{aligned}$$

Here, $\mathcal{E}$ and $\mathcal{L}$ are spatially constant, symmetric second-order strain and stress tensors. Six linear independent loading conditions comprising three plain strain loadings in tension or compression and three shear loadings must be applied to provide volume averaged stress and strain relations which are used to solve for the 21 constitutive constants within the effective elasticity tensor.

*2.1.1. Effective elastic response*

From the elastic relation (3), by taking averages we arrive at the effective material properties of the composite in terms of the effective bulk modulus $\kappa^*$ and effective shear modulus $\mu^*$:

$$\kappa^* \overset{\text{def}}{=} \frac{1}{3}\frac{\left\langle \frac{\text{tr}\boldsymbol{\sigma}}{3}\right\rangle_V}{\left\langle \frac{\text{tr}\boldsymbol{\varepsilon}}{3}\right\rangle_V} \qquad \text{and} \qquad \mu^* \overset{\text{def}}{=} \frac{1}{2}\sqrt{\frac{\langle \boldsymbol{\sigma}'\rangle_V : \langle \boldsymbol{\sigma}'\rangle_V}{\langle \boldsymbol{\varepsilon}'\rangle_V : \langle \boldsymbol{\varepsilon}'\rangle_V}},$$

where $\boldsymbol{\sigma}' \overset{\text{def}}{=} \boldsymbol{\sigma} - \frac{\text{tr}\boldsymbol{\sigma}}{3}\boldsymbol{I}$ is the stress deviator [19]. The effective Young's modulus $E^*$ and elastic Poisson's ratio $\nu^*$ follow from the theory of linear elasticity and are given by

$$E^* \overset{\text{def}}{=} \frac{9\kappa^*\mu^*}{3\kappa^* + \mu^*} \qquad \text{and} \qquad \nu^* \overset{\text{def}}{=} \frac{3\kappa^* - 2\mu^*}{6\kappa^* + 2\mu^*}.$$

*2.1.2. Theoretical bounds*

Historically, homogenization was proposed as a purely analytical process with the simplified models of Voigt [20] and Reuss [21] that gave bounds on the effective moduli. For these models the heterogeneous material was subject to uniform strain or stress. Since neither of these represents the realistic stress/strain states within a complex material, the bounds are not strict except in the very simplest situations [19]. Another important bound is that proposed by Hashin and Shtrikman [22].

*The Voigt and Reuss bounds:.* Voigt [20] and Reuss [21] bounds exist as upper and lower bounds, respectively. In terms of Young's modulus $E$, the bounds for a composite of material 1 and material 2 are given by

$$E_{\text{Voigt}} = \frac{1}{\text{V}}\left[\int_{\text{V}_1} E_1 \text{dV} + \int_{\text{V}_2} E_2 \text{dV}\right] \tag{7}$$

and

$$\frac{1}{E_{\text{Reuss}}} = \frac{1}{\text{V}}\left[\int_{\text{V}_1} \frac{1}{E_1}\text{dV} + \int_{\text{V}_2} \frac{1}{E_2}\text{dV}\right], \tag{8}$$

where $E_1$ and $E_2$ are Young's moduli of material 1 and material 2 respectively. The actual effective modulus lies between these bounds [19], that is,

$$E_{\text{Reuss}} \le E^* \le E_{\text{Voigt}}.$$

*The Hashin–Shtrikman bound:.* Hashin and Shtrikman [22] developed tighter bounds which are based on variational principles. The effective shear and bulk moduli in this model are bounded according to

$$\kappa_1 + \frac{\varphi}{\frac{1}{\kappa_2-\kappa_1} + \frac{3[1-\varphi]}{3\kappa_1+4\mu_1}} \le \kappa^* \le \kappa_2 + \frac{1-\varphi}{\frac{1}{\kappa_1-\kappa_2} + \frac{3\varphi}{3\kappa_2+4\mu_2}} \tag{9}$$

and

$$\mu_1 + \frac{\varphi}{\frac{1}{\mu_2-\mu_1} + \frac{6[1-\varphi][\kappa_1+2\mu_1]}{5\mu_1[3\kappa_1+4\mu_1]}} \le \mu^* \le \mu_2 + \frac{1-\varphi}{\frac{1}{\mu_1-\mu_2} + \frac{6\varphi[\kappa_2+2\mu_2]}{5\mu_2[3\kappa_2+4\mu_2]}}, \tag{10}$$

where $\kappa_1$, $\mu_1$ and $\kappa_2$, $\mu_2$ are the shear and bulk modulus for material 1 and material 2, respectively.

*2.2. Testing methodology*

The homogenization process of the composite is conducted using commercial analysis software, ABAQUS/STANDARD. The material volume element (VE) (Fig. 2) was created by the cutting and merging methods within ABAQUS between a homogeneous block and the pure nanoporous gold structure developed by B.-N. Ngo

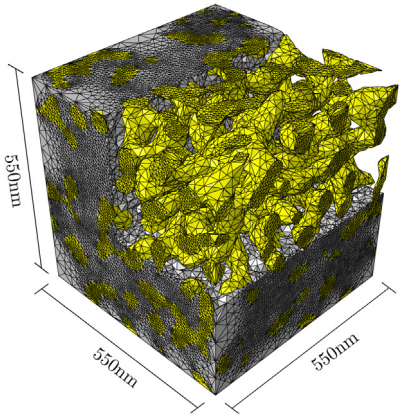


(a)

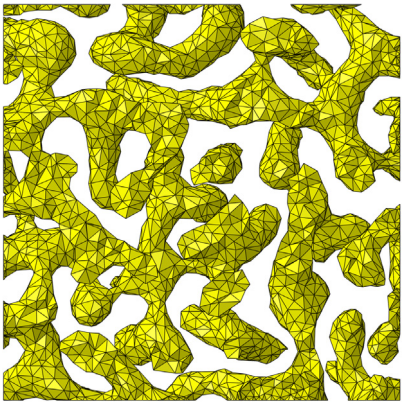

(b)

**Fig. 2.** (a) Volume element of gold–polymer nanocomposite (grey = polymer, yellow = gold) with cut out showing interconnected ligament network. (b) 2D slice of nanoporous gold from VE. (For interpretation of the references to colour in this figure legend, the reader is referred to the web version of this article.)

**Table 1**
Bulk material properties.

| Polymer [25] | Symbol | Value |
|---|---|---|
| Bulk modulus | $\kappa$ | 1.13 GPa |
| Shear modulus | $\mu$ | 0.75 GPa |
| Poisson's ratio | $\nu$ | 0.228 |
| Gold [12] | | |
| Bulk modulus | $\kappa$ | 198.6 GPa |
| Shear modulus | $\mu$ | 27.08 GPa |
| Poisson's ratio | $\nu$ | 0.435 |

(Helmholtz-Zentrum Geesthacht, Germany) [23,24] (the latter was created by imitating spinodal decomposition of a binary mixture using the Metropolis Monte Carlo algorithm). The VE has a gold volume fraction of 29.7% and a relative ligament size of 31.5 nm. No statistical tests were performed to confirm whether this volume element was sufficiently large to correctly represent the infinite material. MESHLAB was used for the mesh creation of 437 913 linear tetrahedral elements. The properties of the constituents are given in Table 1.

*2.2.1. Boundary conditions*

Although the solution converges to the true solution for any boundary condition as the VE size increases, and becomes a representative volume element (RVE), at small VE sizes the effective

property is bounded as follows [26]:

$$E^*_{SU} \leq E^*_P \leq E^*_{KU},$$

with $E^*_{SU}$, $E^*_P$ and $E^*_{KU}$ representing the effective Young's modulus calculated under static uniform, periodic and kinematic uniform boundary conditions respectively.

These bounds are obtained from the principles of minimum potential energy and maximum complementary energy, from which it is shown that kinematic uniform boundary conditions provide a generally stiffer response, while static uniform boundary conditions produce a less stiff response, and the response under periodic boundary conditions generally lies in-between the static and kinematic uniform boundary conditions [27,28].

Periodic boundary conditions are complex to implement, but for a given VE size they provide the best estimate of material properties for both periodic and random VEs [29–31]. Periodic boundary conditions are generally applied by specifying a displacement for the difference between a pair of nodes whose locations correspond to each other but lie on opposite parallel faces of the VE. Thus, Eq. (6c) becomes

$$\boldsymbol{u}^{k+} - \boldsymbol{u}^{k-} = \mathcal{E} \cdot [\mathbf{x}^{k+} - \mathbf{x}^{k-}], \tag{11}$$

where $k+$ and $k-$ represent the kth pair of opposite parallel faces. This can easily be applied via constraint equations between corresponding nodes within the context of the finite element method. Matching nodes thus need to be defined on both faces, and, hence, a periodic mesh is generally required. With complex geometries this is often not possible. Alternative approaches to applying periodic boundary conditions on non-periodic meshes have been developed by various researchers [32,30,33–35].

This work uses the method known as the master/slave approach, proposed by Yuan and Fish [34] and implemented by Schneider et al. [36,37]. It is implemented within Abaqus with the use of the TIE keyword. This keyword involves a slave and master surface where a node on the slave surface is constrained to the movement of the closest node/s on the master surface.

Owing to a limitation in Abaqus however, a boundary condition and a TIE cannot simultaneously be described on one surface. Thus, the master/slave periodic boundary conditions are applied as follows (Fig. 3):

- create a replica of the master surface at a small distance away from the slave surface (blue, yellow and green in Fig. 3),
- place a TIE constraint between the replicated surface and the slave surface,
- apply constraint equations among reference nodes (these are created as external nodes of the VE), replicated master surfaces and the original master surfaces for all degrees of freedom and each associated node (an example for one pair of node sets is shown by the dashed line in Fig. 3),
- apply prescribed displacement to reference point.

## 3. Results and discussion

### 3.1. Numerical homogenization

Numerical homogenization has been carried out on the VE for static uniform, kinematic and periodic boundary conditions, the full elasticity tensor being calculated in each case for six independent loading cases. To quantify the degree of anisotropy in each elasticity tensor anisotropic factors were calculated as follows [38]:

$$Y_{44} = \frac{\mathbb{C}^*_{44} + \mathbb{C}^*_{55} + \mathbb{C}^*_{66}}{3}, \qquad Y_{11} = \frac{\mathbb{C}^*_{11} + \mathbb{C}^*_{22} + \mathbb{C}^*_{33}}{3},$$
$$Y_{12} = \frac{\mathbb{C}^*_{12} + \mathbb{C}^*_{23} + \mathbb{C}^*_{31}}{3}, \quad \text{and} \quad a = \frac{2Y_{44}}{Y_{11} + Y_{12}},$$

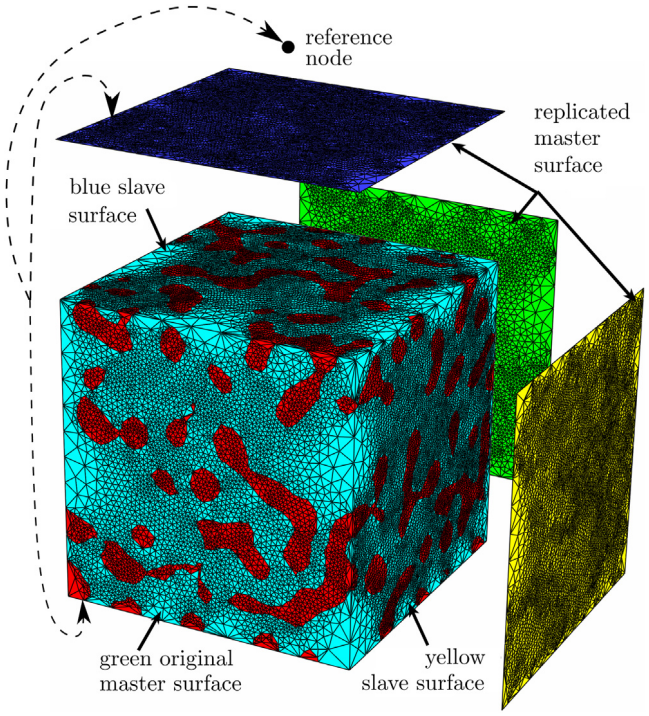


**Fig. 3.** Master/slave set-up for periodic boundary conditions on VE with a non periodic mesh, see also [36,37]. The replicated master surfaces are given by the dark blue, green and yellow surfaces. Tie constraints are created between each replicated surface and corresponding slave surface parallel to it. Additionally constraint equations (dashed line) are developed between corresponding reference nodes, replicated master surfaces the original master surfaces. (For interpretation of the references to colour in this figure legend, the reader is referred to the web version of this article.)

**Table 2**
Effective elastic properties calculated from numerical homogenization under three different boundary conditions.

| Effective property | Boundary condition | | |
|---|---|---|---|
| | Static | Periodic | Kinematic |
| Bulk modulus $\kappa^*$ | 3.717 | 4.417 | 4.381 GPa |
| Shear modulus $\mu^*$ | 2.153 | 2.551 | 2.558 GPa |
| Poisson's ratio $\nu^*$ | 0.257 | 0.258 | 0.255 |
| Young's modulus $E^*$ | 5.413 | 6.417 | 6.423 GPa |

where $a$ is equal to one in a purely isotropic case. This resulted in anisotropic factors in the range of 0.975 to 0.987 indicating a low degree of anisotropy. Thus, the VE is treated as an isotropic material. This allows for only one loading condition to be applied to define the material fully and obtain two effective material parameters.

Uniaxial compression is applied in each of the three major axes separately, with an average effective property then calculated. The results for the effective elastic properties for kinematic uniform, static uniform and periodic boundary conditions are listed in Table 2. Agreement with the ordering of the effective Young's modulus based on the boundary conditions is substantiated by these results, though the kinematic boundary condition gives a result that is only slightly stiffer than the periodic condition. The numerically homogenized results are relatively close to each other, suggesting a good representativeness of the VE to the material at an infinite scale.

The effective Young's modulus is in agreement with that of Wang [39], who experimentally obtained a Young's modulus of 4.01 GPa for a gold–polymer nanocomposite of similar parameter description (volume fraction = 27%, ligament size = 35 nm ±10

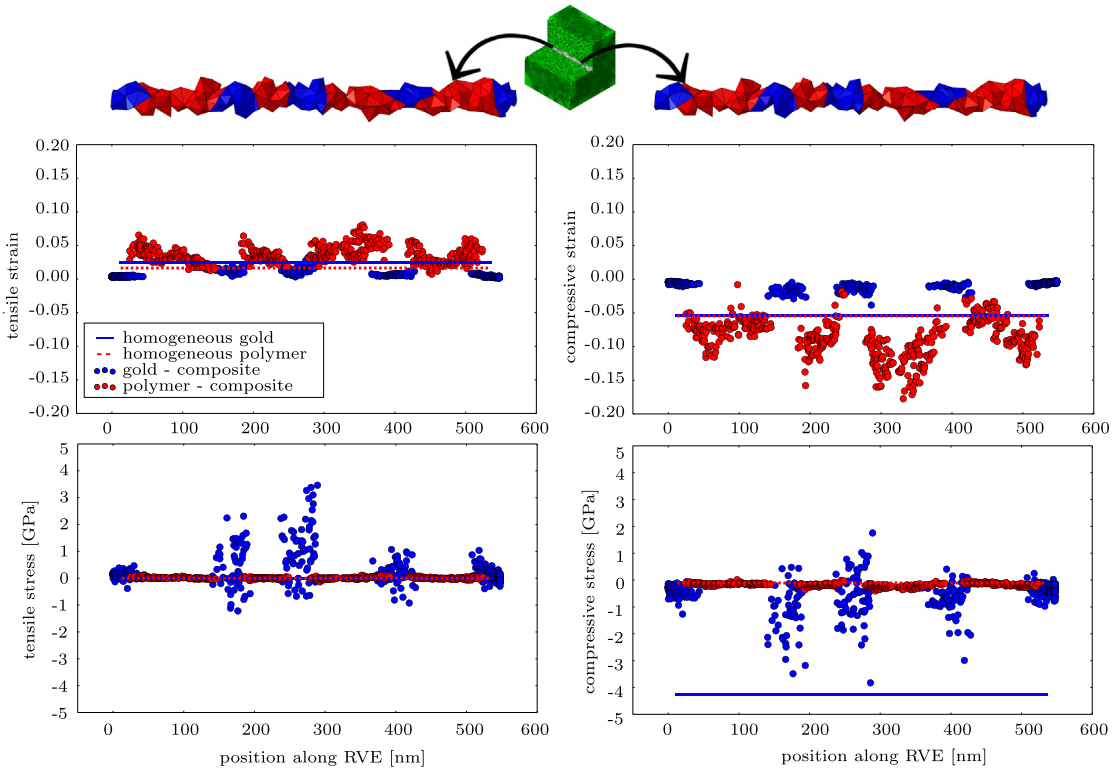


**Fig. 4.** Maximum compressive and tensile stresses and strains along the centroid of the RVE: comparison of bulk gold, bulk polymer, polymer phase in the nanocomposite and gold phase in the nanocomposite. Significantly large tensile stresses and strains are generated in the composite despite simulation of a pure compression test. The gold within the composite shows considerable tensile and compressive stresses of equal magnitude.

nm). Compared to pure nanoporous gold, the composite is slightly stiffer: for example, Balk et al. [12] have given a Young's modulus of 2.7 GPa for a pure sample of nanoporous gold at 30% volume fraction with ligament sizes between 20–30 nm. The Reuss and Voigt bounds for the Young's modulus are calculated as 2.539 and 22.935 GPa, respectively. There is a large range determined by these bounds due to the relatively stiff gold and the conversely highly compliant polymer. The alternate theoretical bounds given by Hashin–Shtrikman are slightly tighter, viz. 3.170 GPa and 14.538 GPa. For all three boundary conditions, the results lie within both the Reuss–Voigt and the Hashin–Shtrikman bounds.

The three numerical results for the effective Young's modulus lie much closer to the lower Reuss average and are close to the middle of the Hashin–Shtrikman bound. The Reuss–Voigt bounds are based on a unidirectional fibre reinforced composite, for which the Reuss average simulates an iso-stress situation of loading normal to the fibre direction. It assumes a matrix (or more compliant material) to carry most of the load, with nominal strengthening being provided by a reinforcement material (or stiffer material). The numerical results are only approximately 15%–20% greater than the Reuss average, thus suggesting that, within the nanocomposite, a large proportion of the strength is provided by the polymer relative to the gold.

### 3.2. Elastic response along centroidal axis

The maximum and minimum compressive and tensile stresses and strains are calculated for a selection of elements located along the RVE's centroidal axis under compression loading specified by a displacement at the boundaries. These stresses and strains are compared to those corresponding to homogeneous blocks of each constituent material undergoing the same loading (Fig. 4). As expected, in the composite the polymer has far higher strains in both compression and tension compared to the gold while the opposite is seen with regard to the stress values. The differing tensile strains between the homogeneous polymer and gold blocks are due to the lateral Poisson's expansion and the differing Poisson's ratios between the two materials. For the homogeneous blocks, the stresses and strains are homogeneous, with only compressive stresses being present.

The polymer in the composite has much larger tensile and compressive strains (0.036 and −0.088) compared to those in the homogeneous polymer block (0.016 and −0.054). The gold shows the opposite trend with lower strains (0.007 and −0.009) compared to gold homogeneous block (0.024 and −0.054 respectively). Despite the loading being compressive, significantly large tensile strains are generated in the composite, due to complex microstructural interactions. However, as expected, the absolute compressive strains are still greater than the tensile ones. To be precise, the maximum compressive strain is slightly more than double the magnitude of the maximum tensile strain. The maximum tensile and compressive stress values along the centroid are however very similar in magnitude (3.46 GPa and −3.83 GPa respectively). A complex interaction between the polymer and gold constituents clearly exists, causing a heterogeneous response with high tensile stresses during compressive loading.

The gold within the composite exhibits significantly lower values of compressive stresses than those corresponding to the homogeneous block. The polymer shows marginally higher stress values within the composite compared to the pure polymer block. This suggests a load transfer between the gold and polymer material to allow for lower stress values.

### 3.3. Loading case of the ligaments

The resultant stress distributions on the cross sections of 10 different ligaments within the composite are analysed under compression loading along the $x$-axis, with a view to determining the

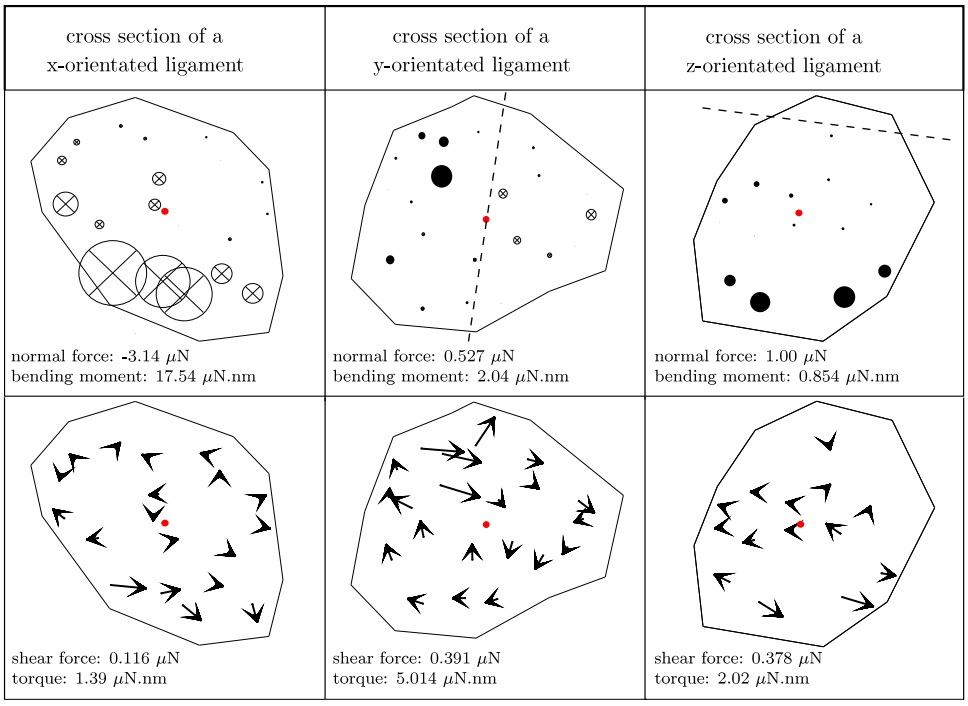


**Fig. 5.** Normal and shear stress distribution on the cross section of three ligaments with in the RVE. — — = approximate bending neutral axis of *y* and *z*-orientated ligaments. ⊗ = inward pointing normal force, • = outward pointing normal force calculated at each elemental centroid. Where the diameter of the circle or length of line represents the relative magnitude of the normal or shear force respectively. • = centroid of ligament cross section.

**Table 3**
Average loading mode magnitudes for 10 ligaments.

| Loading mode | Value |
|---|---|
| Bending moment | 4.255 μN·nm |
| Torque | 2.279 μN·nm |
| Normal force | 1.233 μN |
| Shear force | 0.229 μN |

dominant modes of stress at the selected locations. Six of the ligaments lie along the major axes of the RVE and four ligaments lie at random orientations. The traction vector, bending moment and torque are calculated on each cross-section, which constitutes a plane normal to the centroidal axis of the ligament. The values were calculated at the centroid of every element lying on this plane.

The average values of the 10 ligaments for each loading mode (Table 3) indicate that bending is the dominant loading case. Nevertheless, the magnitudes of the torque and normal forces are still significant. Shear stress is more prevalent than expected as it is only one order of magnitude less than the normal force. Ligaments lying at random orientations show no clear trend in dominant loading cases and are, therefore, not discussed further.

The normal and shear stress distribution of three sample ligaments lying along each axis are shown in Fig. 5. Very little difference is seen in the normal and shear stress distributions between ligaments along the same axis.

The stress distribution of the ligament along the axis of compression shows a combination of both compression and bending. A far greater normal force and bending moment are also experienced by the ligament aligned with the compression axis, compared to those having different orientations. The presence of significant normal forces through all ligaments with a shift in the bending neutral axis is evident in two ligaments and is in accord with the experimental observation of Wang and Weissmüller [4]. Thus showing agreement that there is a different loading case in the composite ligaments compared to the pure nanoporous gold ligaments. It is also in some agreement with the finding of Bargmann et al. [15] who found high compression/tension stresses for ligaments along the compressive axis.

Bending is clearly seen on all three normal stress distributions in Fig. 5, as seen by the magnitude of the normal stress decreasing along the cross-section of the ligament. The ligament in the direction of compression has normal forces acting into the cross-section only, giving a high resultant normal force, whereas normal stress distributions of ligaments not along this axis have a dense region of forces acting out of the cross-section which decrease and change into forces acting into the cross-section along the ligament cross-section. Deshpande et al. [40] state that a tension/compression-dominant foam is expected to be much stiffer and stronger than one in which bending dominates. Although the Gibson–Ashby [41] foam scaling equations are known to be inappropriate for prediction of the strength and stiffness of nanoporous gold [16,14], the underlying principles still apply. That is, the strength and stiffness of a foam scales with the relative density much faster for foams with tension/compression dominated deformation. Thus, at the same relative density, a tension/compression deformation dominated material will be much stronger than one in which bending dominates. The increased stiffness shown in Section 3.1 compared to that for the pure nanoporous gold sample may thus arise not only as a result of the addition of the polymer, but also due to the shift in loading case. The tension–compression symmetry shown in this model suggests that the nanocomposite shows the same loading modes in tension as in compression. The significant presence of bending and not only normal forces in the ligaments may thus account for the enhanced ductility. The presence of tension/compression loading modes allows for enhancement of strength without high stiffness due to the presence of the bending loading mode. Additionally, it suggests that by increasing the amount of tension/compression through fine-tuning the microstructure, materials with design specific properties could be created.

In contrast to the normal stress, the shear stress distribution shows almost no clear trend in any of the ligaments monitored. However, a small region of higher shear forces is seen on one edge in each ligament in Fig. 5. There are also greater shear forces on the outer edges of the ligament surface: these are suggestive of torsional stresses. The high torque experienced by the ligament orientated normal to the direction of compression is clearly seen in the circular trend of shear forces on the ligament face in Fig. 5. The presence of significant shear forces and torque suggests a complex interaction at the interface between the gold and polymer. Behaviour at these interfaces play a significant role in the determining unique characteristics of the material (see also Wilmers et al. [1] and Elsner et al. [2]), while the possibility of delamination as a main deformation mechanism can also not be ruled out due to the high surface-to-volume ratio of nanoporous gold.

## 4. Conclusion

Nanoporous metals have gain in popularity as the basic ingredient for high-performance composites [42–44]. Tailor made materials with custom designed mechanical properties, including overcoming of what seemed to hold true for all materials, i.e., increasing strength accompanied by reduced damage tolerance and greater brittleness, are the goal. Gold serves as a model material in the ongoing analyses of the properties of nanoporous metals (and their composite counterparts) because it is insensitive to most impurities. Research on how to substitute gold with less exclusive metals is continuously growing. To date, even the most basic property, i.e., the elastic behaviour of such nanocomposites, is not fully understood at the nanoscale.

This study was concerned with an analysis via numerical homogenization of an RVE of a linear elastic gold–polymer nanocomposite comprising ligaments of 31.5 nm in diameter and with a ∼30% gold volume fraction. The resulting effective Young's modulus varies between 5.4 and 6.4 GPa, values that lie well within both the Reuss–Voigt and Hashin–Shtrikman bounds. The elastic response along the centroid of the RVE showed significant compressive and tensile behaviour existing within the composite even if only under compressive loading. The gold within the composite showed considerable tensile and compressive stresses of equal magnitude. All ligaments showed clear trends of combined bending, torsion, and normal forces. The dominant loading case was bending with torsion, normal force and shear force present in descending order of magnitude. The ligaments aligned along the compression axis showed much higher normal forces and bending moments compared to those aligned along the other two axes. Randomly oriented ligaments showed no clear trend in their dominant loading case. The shear stress showed little to no clear trend in distribution, though it did contribute to the high shear forces and torques experienced by the ligaments. The increased stiffness of a gold–polymer nanocomposite is achieved by filling the pores of nanoporous gold with polymer. Hereby, with respect to stiffness, the contribution of the additional material is reduced by a shift in loading case from compression/tension to bending with torsion.

By fine-tuning the microstructure by reducing the amount of bending in the ligaments (and increasing the amount of tension/compression), even better mechanical properties should be achieved.

## Acknowledgements

SB gratefully acknowledges financial support from the German Research Foundation (DFG) via SFB 986 "M$^3$", project B6. Part of this research was done while SB visited the Centre for Research in Computational and Applied Mechanics, University of Cape Town, whose hospitality is gratefully acknowledged. BDR and EG acknowledge the support of the National Research Foundation (grant number 47584) through the South African Research Chair in Computational Mechanics. The authors thank Dr. Celal Soyarslan (University of Wuppertal, Germany) for the transformation of the point cloud data into the finite-element model of the pure nanoporous gold structure used in this study and K. Schneider (Hamburg University of Technology, Germany) for assisting with the implementation of master–slave periodic boundary conditions.

## References

[1] J. Wilmers, A. McBride, S. Bargmann, Interface elasticity effects in polymer-filled nanoporous metals, J. Mech. Phys. Solids 99 (2017) 163–177. http://dx.doi.org/10.1016/j.jmps.2016.11.011.
[2] B. Elsner, S. Müller, S. Bargmann, J. Weissmüller, Surface excess elasticity of gold: ab initio coefficients and impact on the effective elastic response of nanowires, Acta Mater. 124 (2017) 468–477. http://dx.doi.org/10.1016/j.actamat.2016.10.066.
[3] J. Biener, A.M. Hodge, J.R. Hayes, C.A. Volkert, L.A. Zepeda-Ruiz, A.V. Hamza, F.F. Abraham, Size effects on the mechanical behavior of nanoporous Au, Nano Lett. 6 (10) (2006) 2379–2382. http://dx.doi.org/10.1021/nl061978i.
[4] K. Wang, J. Weissmüller, Composites of nanoporous gold and polymer, Adv. Mater. 25 (9) (2013) 1280–1284. http://dx.doi.org/10.1002/adma.201203740.
[5] H.-J. Jin, L. Kurmanaeva, J. Schmauch, H. Rösner, Y. Ivanisenko, J. Weissmüller, Deforming nanoporous metal: role of lattice coherency, Acta Mater. 57 (9) (2009) 2665–2672. http://dx.doi.org/10.1016/j.actamat.2009.02.017.
[6] A. Wittstock, J. Biener, J. Erlebacher, M. Baumer (Eds.), Nanoporous Gold, Royal Society of Chemistry Nanoscience & Nanotechnology, The Royal Society of Chemistry, 2012. http://dx.doi.org/10.1039/9781849735285.
[7] Y. Ding, M. Chen, J. Erlebacher, Metallic mesoporous nanocomposites for electrocatalysis, J. Am. Chem. Soc. 126 (22) (2004) 6876–6877. http://dx.doi.org/10.1021/ja0320119.
[8] S. Kucheyev, J. Hayes, J. Biener, T. Huser, C. Talley, A. Hamza, Surface-enhanced Raman scattering on nanoporous Au, Appl. Phys. Lett. 89 (5) (2006) 053102. http://dx.doi.org/10.1063/1.2260828.
[9] H.-J. Jin, J. Weissmüller, Bulk nanoporous metal for actuation, Adv. Energy Mater. 12 (8) (2010) 714–723. http://dx.doi.org/10.1002/adem.200900329.
[10] J. Biener, A.M. Hodge, A.V. Hamza, Microscopic failure behavior of nanoporous gold, Appl. Phys. Lett. 87 (12) (2005) 121908. http://dx.doi.org/10.1063/1.2051791.
[11] J. Weissmüller, R.C. Newman, H.-J. Jin, A.M. Hodge, J.W. Kysar, Nanoporous metals by alloy corrosion: formation and mechanical properties, Mater. Res. Soc. Bull. 34 (08) (2009) 577–586. http://dx.doi.org/10.1557/mrs2009.157.
[12] T.J. Balk, C. Eberl, Y. Sun, K.J. Hemker, D.S. Gianola, Tensile and compressive microspecimen testing of bulk nanoporous gold, J. Miner. Met. Mater. Soc. 61 (12) (2009) 26–31. http://dx.doi.org/10.1007/s11837-009-0176-6.
[13] N.J. Briot, T. Kennerknecht, C. Eberl, T.J. Balk, Mechanical properties of bulk single crystalline nanoporous gold investigated by millimetre-scale tension and compression testing, Philos. Mag. 94 (8) (2014) 847–866. http://dx.doi.org/10.1080/14786435.2013.868944.
[14] N. Huber, R. Viswanath, N. Mameka, J. Markmann, J. Weissmüller, Scaling laws of nanoporous metals under uniaxial compression, Acta Mater. 67 (2014) 252–265. http://dx.doi.org/10.1016/j.actamat.2013.12.003.
[15] S. Bargmann, C. Soyarslan, E. Husser, N. Konchakova, Materials based design of structures: Computational modeling of the mechanical behavior of gold-polymer nanocomposites, Mech. Mater. 94 (2016) 53–65. http://dx.doi.org/10.1016/j.mechmat.2015.11.008.
[16] L. Lührs, C. Soyarslan, J. Markmann, S. Bargmann, J. Weissmüller, Elastic and plastic Poisson's ratios of nanoporous gold, Scr. Mater. 110 (2016) 65–69. http://dx.doi.org/10.1016/j.scriptamat.2015.08.002.
[17] K. Wang, A. Kobler, C. Kübel, H. Jelitto, G. Schneider, J. Weissmüller, Nanoporous-gold-based composites: toward tensile ductility, NPG Asia Mater. 7 (6) (2015) e187. http://dx.doi.org/10.1038/am.2015.58.
[18] R. Hill, The elastic behaviour of a crystalline aggregate, Proc. Phys. Soc. A 65 (5) (1952) 349. http://dx.doi.org/10.1088/0370-1298/65/5/307.
[19] T.I. Zohdi, P. Wriggers, An Introduction to Computational Micromechanics, Springer Science & Business Media, 2008, pp. 45–62 Ch. 4.
[20] W. Voigt, Ueber die beziehung zwischen den beiden elasticitätsconstanten isotroper körper, Ann. Phys. 274 (12) (1889) 573–587.
[21] A. Reuss, Berechnung der Fließgrenze von Mischkristallen auf grund der Plastizitätsbedingung für Einkristalle, Z. Angew. Math. Mech. 9 (1) (1929) 49–58.
[22] Z. Hashin, S. Shtrikman, A variational approach to the theory of the elastic behaviour of multiphase materials, J. Mech. Phys. Solids 11 (2) (1963) 127–140. http://dx.doi.org/10.1016/0022-5096(63)90060-7.
[23] B.-N.D. Ngô, A. Stukowski, N. Mameka, J. Markmann, K. Albe, J. Weissmüller, Anomalous compliance and early yielding of nanoporous gold, Acta Mater. 93 (2015) 144–155. http://dx.doi.org/10.1016/j.actamat.2015.04.021.

[24] B.-N.D. Ngô, B. Roschning, K. Albe, J. Weissmüller, J. Markmann, On the origin of the anomalous compliance of dealloying-derived nanoporous gold, Scr. Mater. 130 (2017) 74–77. http://dx.doi.org/10.1016/j.scriptamat.2016.11.006.
[25] T.V. Vernitskaya, O.N. Efimov, Polypyrrole: a conducting polymer; its synthesis, properties and applications, Russ. Chem. Rev. 66 (5) (1997) 443. http://dx.doi.org/10.1070/RC1997v066n05ABEH000261.
[26] M. Jiang, I. Jasiuk, M. Ostoja-Starzewski, Apparent elastic and elastoplastic behavior of periodic composites, Int. J. Solids Struct. 39 (1) (2002) 199–212. http://dx.doi.org/10.1016/S0020-7683(01)00145-7.
[27] S.J. Hollister, N. Kikuchi, A comparison of homogenization and standard mechanics analyses for periodic porous composites, Comput. Mech. 10 (2) (1992) 73–95. http://dx.doi.org/10.1007/BF00369853.
[28] M. Hori, S. Nemat-Nasser, On two micromechanics theories for determining micro–macro relations in heterogeneous solids, Mech. Mater. 31 (10) (1999) 667–682. http://dx.doi.org/10.1016/S0167-6636(99)00020-4.
[29] T. Kanit, S. Forest, I. Galliet, V. Mounoury, D. Jeulin, Determination of the size of the representative volume element for random composites: statistical and numerical approach, Int. J. Solids Struct. 40 (13) (2003) 3647–3679. http://dx.doi.org/10.1016/S0020-7683(03)00143-4.
[30] F. Larsson, K. Runesson, S. Saroukhani, R. Vafadari, Computational homogenization based on a weak format of micro-periodicity for RVE-problems, Comput. Methods Appl. Mech. Engrg. 200 (1) (2011) 11–26. http://dx.doi.org/10.1016/j.cma.2010.06.023.
[31] K. Terada, M. Hori, T. Kyoya, N. Kikuchi, Simulation of the multi-scale convergence in computational homogenization approaches, Int. J. Solids Struct. 37 (16) (2000) 2285–2311. http://dx.doi.org/10.1016/S0020-7683(98)00341-2.
[32] G.A. Kassem, Micromechanical material models for polymer composites through advanced numerical simulation techniques, Aachen University, Germ any, 2009, Ph.D. thesis.
[33] J. Tyrus, M. Gosz, E. DeSantiago, A local finite element implementation for imposing periodic boundary conditions on composite micromechanical models, Int. J. Solids Struct. 44 (9) (2007) 2972–2989. http://dx.doi.org/10.1016/j.ijsolstr.2006.08.040.
[34] Z. Yuan, J. Fish, Toward realization of computational homogenization in practice, Internat. J. Numer. Methods Engrg. 73 (3) (2008) 361–380. http://dx.doi.org/10.1002/nme.2074.
[35] V.-D. Nguyen, E. Béchet, C. Geuzaine, L. Noels, Imposing periodic boundary condition on arbitrary meshes by polynomial interpolation, Comput. Mater. Sci. 55 (2012) 390–406. http://dx.doi.org/10.1016/j.commatsci.2011.10.017.
[36] K. Schneider, B. Klusemann, S. Bargmann, Fully periodic RVEs for technological relevant composites:not worth the effort! J. Mech. Mater. Struct. http://dx.doi.org/10.2140/jomms.2017.12.471.
[37] K. Schneider, B. Klusemann, S. Bargmann, Automatic three-dimensional geometry and mesh generation of periodic representative volume elements for matrix-inclusion composites, Adv. Eng. Softw. 99 (2016) 177–188. http://dx.doi.org/10.1016/j.advengsoft.2016.06.001.
[38] T. Kanit, F. N'Guyen, S. Forest, D. Jeulin, M. Reed, S. Singleton, Apparent and effective physical properties of heterogeneous materials: representativity of samples of two materials from food industry, Comput. Methods Appl. Mech. Engrg. 195 (33) (2006) 3960–3982. http://dx.doi.org/10.1016/j.cma.2005.07.022.
[39] K. Wang, Composites of nanoporous gold and polymer, Technischen Universität, Hamburg, 2015, Ph.D. thesis.
[40] V. Deshpande, M. Ashby, N. Fleck, Foam topology: bending versus stretching dominated architectures, Acta Mater. 49 (6) (2001) 1035–1040. http://dx.doi.org/10.1016/S1359-6454(00)00379-7.
[41] L. Gibson, M. Ashby, Cellular Solids: Structure and Properties, in: Cambridge Solid State Science Series, Cambridge University Press, 1999.
[42] H.-J. Jin, J. Weissmüller, A material with electrically tunable strength and flow stress, Science 332 (6034) (2011) 1179–1182. http://dx.doi.org/10.1126/science.1202190.
[43] I. Okulov, J. Weissmüller, J. Markmann, Dealloying-based interpenetrating-phase nanocomposites matching the elastic behavior of human bone, Sci. Rep. 7 (1) (2017) 20. http://dx.doi.org/10.1038/s41598-017-00048-4.
[44] Q. Kong, L. Lian, Y. Liu, J. Zhang, L. Wang, W. Feng, Bulk hierarchical nanoporous palladium prepared by dealloying pdal alloys and its electrochemical properties, Microporous Mesoporous Mater. 208 (2015) 152–159. http://dx.doi.org/10.1016/j.micromeso.2015.01.017.